

# Vortices in spinor cold exciton condensates with spin-orbit interaction

H. Sigurdsson,<sup>1,2</sup> T. C. H. Liew,<sup>1</sup> O. Kyriienko,<sup>1,2</sup> and I. A. Shelykh<sup>1,2</sup>

<sup>1</sup>*Division of Physics and Applied Physics, Nanyang Technological University 637371, Singapore*

<sup>2</sup>*Science Institute, University of Iceland, Dunhagi-3, IS-107, Reykjavik, Iceland*

(Dated: November 4, 2018)

We study theoretically the ground states of topological defects in a spinor four-component condensate of cold indirect excitons. We analyze possible ground state solutions for different configurations of vortices and half-vortices. We show that if only Rashba or Dresselhaus spin-orbit interaction (SOI) for electrons is present the stable states of topological defects can represent a cylindrically symmetric half-vortex or half vortex-antivortex pairs, or a non-trivial pattern with warped vortices. In the presence of both of Rashba and Dresselhaus SOI the ground state of a condensate represents a stripe phase and vortex type solutions become unstable.

PACS numbers: 71.35.Lk, 03.75.Mn, 71.70.Ej

## I. INTRODUCTION

An existence of topological phases and excitations can be seen as a manifestation of unique and universal laws of physics. Being widely studied in various systems, a remarkable understanding of topological defects was attained for Bose-Einstein condensates of ultracold atoms,<sup>1,2</sup> where quantization of angular momentum was experimentally observed.<sup>3</sup> The resulting quasi-particles — quantum vortices — consist of a vortex core, where the condensate density reaches its minimum and phase becomes singular, and a circulating superfluid flow around, with phase winding being an integer number of  $2\pi$ .<sup>4</sup> Other examples of topological defects include domain walls, solitons,<sup>5</sup> warped vortices,<sup>6</sup> skyrmions,<sup>7</sup> and fractional vortices which can appear in multicomponent<sup>8</sup> or spinor condensate systems.<sup>9</sup>

The usual scheme for generation of vortices in atomic physics is based on the effective Lorentz force appearing due to rotation of the condensate.<sup>10,11</sup> Recently an alternative approach with an optically-induced artificial gauge field generation was realized.<sup>12</sup> The next important step forward in manipulation of atomic condensates was performed with implementation of an artificial spin-orbit coupling between several spin components.<sup>13</sup> Followed by numerous theoretical proposals,<sup>14–16</sup> this system was shown to be an excellent playground for studying diverse spin-related topological phases and excitations,<sup>17</sup> including single plane wave and striped phases,<sup>18</sup> hexagonally-symmetric phase,<sup>19</sup> square vortex lattice,<sup>20</sup> skyrmion lattice,<sup>21</sup> and even a quasicrystalline phase for cold dipolar bosons.<sup>22</sup>

A major drawback in the study of cold atom systems is the ultralow temperature ( $< 1$  nK) required for condensation of atoms in magnetic traps. However, solid-state physics offers a large variety of systems, where bosonic quasiparticles with small effective mass can condense at comparably high temperatures. They include Quantum Hall bilayers,<sup>23</sup> magnons,<sup>24</sup> indirect excitons,<sup>25–27</sup> and cavity exciton-polaritons.<sup>28–31</sup> Moreover, the latter system possesses a spinor structure being formed by two po-

lariton spin components with  $\pm 1$  spin projection.<sup>32</sup> Complementary to the full quantum vortices in the polariton fluids,<sup>33–35</sup> this allows one to study half-integer quantum vortices<sup>36–38</sup> and their warped analogs.<sup>6,36,39</sup> An intriguing spin dynamics there is caused by an analog of spin-orbit interaction (SOI) given by momentum-dependent TE-TM splitting.<sup>40–42</sup>

Even higher spin degeneracy can be achieved for the system of indirect excitons — bound pairs of electrons and holes which are spatially separated in two parallel quantum wells [Fig. 1].<sup>43–45</sup> Due to the small overlap between the wavefunctions of electrons and holes these quasiparticles possess very large radiative lifetime (up to microseconds), which allows them to thermalize and consequently form a macroscopically coherent state with properties similar to a Bose-Einstein condensate.<sup>27</sup> Another important feature of indirect exciton gases is formation of a so-called macroscopically ordered state manifesting itself as a fragmented exciton ring.<sup>46–48</sup>

Accounting for four possible  $\pm 1, \pm 2$  cold indirect exciton spin projections, an ambiguous choice of condensate ground state is possible.<sup>49,50</sup> This results in non-trivial condensate topology and the possibility for generation of various topological defects.<sup>51</sup> Moreover, complex spin textures around fragmented beads of cold exciton condensates were observed.<sup>52</sup> They were explained with an influence of SOI of various types, which affects the center-of-mass exciton motion.<sup>50,53,54</sup> This assures that physics similar to atomic spin-orbit coupled condensates, including artificial magnetic field generation,<sup>55</sup> can be studied with cold indirect excitons.

In this paper we study the ground states of various topological defects in an indirect exciton condensate. We show that the presence of the SOI leads to drastic changes in the ground state of the topological defects in the indirect exciton condensate. Using the imaginary-time Gross-Pitaevskii equations for the spinor macroscopic wave function, we find that in the presence of only one type of SOI half-vortex solutions are possible, while for both Rashba and Dresselhaus SOI the only possible stable solution is a striped state with zero vorticity. We study the numerical solutions of the equations and de-

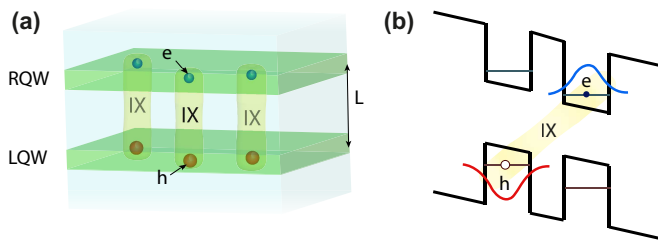


FIG. 1: (Color online) Sketch of the system. (a) A heterostructure with biased coupled quantum wells, where an electron from the right quantum well (RQW) is coupled with a heavy hole in the left quantum well (LQW), forming an indirect exciton (IX). (b) The energy structure of an electron-hole bilayer showing spatial separation of electron (e) and hole (h) wave functions.

rive analytical estimates for the boundaries, which define topological charge stabilities. The results are consistent with recent experimental observations of spin textures in a diluted coherent gas of cold indirect excitons.

## II. THE MODEL

An indirect exciton is a composite boson consisting of a spatially separated electron and hole [Fig. 1]. Its spin is defined by electron and heavy hole spin projections on the structure growth axis, being  $\pm 1/2$  and  $\pm 3/2$ , respectively. The resulting four combinations correspond to possible exciton spin projections,  $S_z = \pm 1, \pm 2$ . The states with  $S_z = \pm 1$  are called the bright excitons, since they can be optically excited by an external pump. In contrast, the states with  $S_z = \pm 2$  spin are optically inactive due to angular momentum conservation selection rules and are typically referred to as dark excitons. However, they can appear due to exchange interaction between bright states or as a result of spin-orbit interaction. In the case of direct excitons the bright and dark states are typically split by short range electron-hole exchange, with dark states lying at lower energies.<sup>56</sup> This can possibly lead to the dark or gray condensation in the corresponding systems, which prevents direct observation of macroscopic coherence in the photoluminescence measurements.<sup>57,58</sup> Moreover, the effects of spin-orbit interactions were shown to interplay with a bright-dark splitting, leading to unconventional pairing effects in the dense BCS-like direct exciton condensates.<sup>59</sup> In the case of indirect excitons the small overlap between electron and hole wave functions leads to approximately equal energies of all four indirect exciton states. The dark states still play an important role and cannot be excluded from the consideration.<sup>60,61</sup>

To describe a coherent state of indirect excitons, we can use the mean-field treatment similar to Refs. [50,51], where the Gross-Pitaevskii equation for the four-component wave function  $\Psi = (\Psi_{+2}, \Psi_{+1}, \Psi_{-1}, \Psi_{-2})$  was introduced. In the general form it can be derived varying

the Hamiltonian density over the macroscopic wave function,  $i\hbar d\Psi/dt = \partial\mathcal{H}/\partial\Psi^*$ . The Hamiltonian density can be written as a sum of a linear single particle and nonlinear interaction parts,  $\mathcal{H} = \mathcal{H}_0 + \mathcal{H}_{\text{int}}$ .

The single particle part of the Hamiltonian density is composed of the kinetic energy and SOI. The latter appears as a consequence of spin-orbit interaction acting on the electron or hole spin. In the following we will account only for the part of SOI affecting the spin of electron. It consists of two terms. The Dresselhaus term arises from bulk inversion asymmetry and for a [001] quantum well is described by the Hamiltonian  $H_D = \beta(\sigma_x k_x - \sigma_y k_y)$ , where  $k_{x,y}$  are Cartesian components of the electron wave vector,  $\sigma_{x,y}$  are Pauli matrices, and  $\beta$  denotes the strength of the Dresselhaus interaction. The Rashba term appears due to structure inversion asymmetry and is described by the Hamiltonian  $H_R = \alpha(\sigma_x k_y - \sigma_y k_x)$ , with  $\alpha$  being the strength of the Rashba interaction.

The single particle term in the Hamiltonian density thus reads<sup>50</sup>:

$$\mathcal{H}_0 = \Psi^\dagger \hat{\mathbf{T}} \Psi, \quad (1)$$

where

$$\hat{\mathbf{T}} = \begin{pmatrix} \hat{\mathbf{T}}_0 & \emptyset \\ \emptyset & \hat{\mathbf{T}}_0 \end{pmatrix}, \quad (2)$$

with  $\emptyset$  being a null matrix and

$$\hat{\mathbf{T}}_0 = \begin{pmatrix} \hbar^2 K^2 / 2m_X & S_K \\ S_K^* & \hbar^2 K^2 / 2m_X \end{pmatrix}. \quad (3)$$

Here

$$S_K = \chi[\beta(K_x + iK_y) + \alpha(K_y + iK_x)], \quad (4)$$

where  $\chi = m_e/m_X$  is the electron-to-exciton mass ratio and  $K = -i\nabla$  denotes the center of mass wave vector of the indirect exciton. Note that in the described Hamiltonian we neglect the bright-dark splitting of the indirect exciton states. This however can be straightforwardly introduced for the systems, where such a splitting was observed.<sup>54,58</sup>

The nonlinear part of the Hamiltonian density  $H_{\text{int}}$  describes interactions between indirect excitons. Since excitons are composite bosons, there are four possible types of interactions corresponding to the exchange of electrons ( $V_e$ ), exchange of holes ( $V_h$ ), simultaneous exchange of electron and hole (or exciton exchange,  $V_X$ ), and direct Coulomb repulsion ( $V_{\text{dir}}$ ). Introducing the interaction constants  $V_0 = V_e + V_h + V_{\text{dir}} + V_X$  and  $W = V_e + V_h$ , the interaction part of the Hamiltonian density becomes

$$\begin{aligned} \mathcal{H}_{\text{int}} = & \frac{V_0}{2} (|\Psi_{+2}|^2 + |\Psi_{+1}|^2 + |\Psi_{-1}|^2 + |\Psi_{-2}|^2)^2 \\ & + W (\Psi_{+1}^* \Psi_{-1}^* \Psi_{+2} \Psi_{-2} + \Psi_{+2}^* \Psi_{-2}^* \Psi_{+1} \Psi_{-1}) \\ & - W (|\Psi_{+2}|^2 |\Psi_{-2}|^2 + |\Psi_{+1}|^2 |\Psi_{-1}|^2). \end{aligned} \quad (5)$$

We mainly focus on the weakly depleted Bose-Einstein condensates of indirect excitons where the biggest interaction contribution comes from vanishing transferred momentum  $q$ , thus working in the long wavelength limit ( $q \rightarrow 0$ ), where  $V_{\text{dir}} = V_X$  and  $V_e = V_h$  (s-wave approximation). The interaction parameters can be further estimated using a narrow QW approximation.<sup>50</sup>

As a specific system corresponding to our model we consider the indirect exciton system studied in Ref. [27],

where macroscopic coherence of indirect exciton gas was reported. The studied sample is high quality double quantum well structure with 8 nm GaAs QWs and a 4 nm  $\text{Al}_{0.33}\text{Ga}_{0.67}\text{As}$  barrier. The observation of nontrivial spin structures in the same sample presumes an importance of spin-orbit interaction in the described system.<sup>52</sup>

The dynamics of the system is described by a set of four coupled nonlinear equations of Gross-Pitaevskii type:

$$i\hbar \frac{\partial \Psi_{+2}}{\partial t} = \hat{E}\Psi_{+2} + \hat{S}_R \Psi_{+1} + V_0 \Psi_{+2} |\Psi_{+2}|^2 + (V_0 - W) \Psi_{+2} |\Psi_{-2}|^2 + V_0 \Psi_{+2} (|\Psi_{-1}|^2 + |\Psi_{+1}|^2) + W \Psi_{-2}^* \Psi_{+1} \Psi_{-1}, \quad (6)$$

$$i\hbar \frac{\partial \Psi_{+1}}{\partial t} = \hat{E}\Psi_{+1} - \hat{S}_R^* \Psi_{+2} + V_0 \Psi_{+1} |\Psi_{+1}|^2 + (V_0 - W) \Psi_{+1} |\Psi_{-1}|^2 + V_0 \Psi_{+1} (|\Psi_{-2}|^2 + |\Psi_{+2}|^2) + W \Psi_{-1}^* \Psi_{+2} \Psi_{-2}, \quad (7)$$

$$i\hbar \frac{\partial \Psi_{-1}}{\partial t} = \hat{E}\Psi_{-1} + \hat{S}_R \Psi_{-2} + V_0 \Psi_{-1} |\Psi_{-1}|^2 + (V_0 - W) \Psi_{-1} |\Psi_{+1}|^2 + V_0 \Psi_{-1} (|\Psi_{+2}|^2 + |\Psi_{-2}|^2) + W \Psi_{+1}^* \Psi_{+2} \Psi_{-2}, \quad (8)$$

$$i\hbar \frac{\partial \Psi_{-2}}{\partial t} = \hat{E}\Psi_{-2} - \hat{S}_R^* \Psi_{-1} + V_0 \Psi_{-2} |\Psi_{-2}|^2 + (V_0 - W) \Psi_{-2} |\Psi_{+2}|^2 + V_0 \Psi_{-2} (|\Psi_{+1}|^2 + |\Psi_{-1}|^2) + W \Psi_{+2}^* \Psi_{+1} \Psi_{-1}. \quad (9)$$

Here  $\hat{E} = -\hbar^2 \nabla^2 / 2m_X$  is the exciton kinetic energy operator and

$$\hat{S}_R = \chi \left[ \beta (\hat{\partial}_y - i\hat{\partial}_x) + \alpha (\hat{\partial}_x - i\hat{\partial}_y) \right] \quad (10)$$

is the SOI operator accounting for both Rashba ( $\alpha$ ) and Dresselhaus ( $\beta$ ) contributions.

### III. NUMERICAL METHOD

We use the imaginary time method to find the state corresponding to the local minima of the Hamiltonian of the interacting exciton system described by Eqs. (6)-(9). Fourier spectral methods are used in space and a variable order Adams-Bashforth-Moulton method in time to achieve accurate discrete gradient flow towards a possible low energy state. Note, that the energy profile can have multiple minima, and the one that is reached in numerical procedure strongly depends on the initial conditions. In particular, one can suppose that if a stable vortex is present in the system the corresponding solution will be found if the initial distribution contains non-zero vorticity, while the ground state with zero vorticity (homogeneous or striped) will be found if one does not have an initial angular momentum. If the system does not possess any stable solutions in the form of vortices, state with no angular momentum will be recovered independently of the initial condition.

We introduce a weak harmonic 2D-trapping potential  $V_{\text{trap}}$  in the Hamiltonian to keep the condensate localized within the system. The trap profile is given by  $V_{\text{trap}} = u_0 \mathbf{r}_\perp^2$ , where  $u_0 = m_X \omega^2 / 2$  represents the trap strength.

A choice of initial conditions is not always trivial when dealing with a nonlinear set of equations controlled by many parameters. In our case the typical initial condition corresponds to the vortex solution:

$$\Psi_\sigma(\mathbf{r}) = R^{(0)}(r) \frac{r/\chi}{\sqrt{r^2/\chi^2 + 1}} e^{i(m_\sigma \theta + k_\sigma \pi)}. \quad (11)$$

Here  $R^{(0)}(r)$  is a Gaussian function corresponding to the trapped exciton gas,  $\sigma$  is the spin index and  $\chi$  is the healing length of the vortex in a one component BEC given by  $\chi = \hbar / \sqrt{2m_X V_0 n}$ ,<sup>62</sup> where  $V_0$  is the nonlinear interaction parameter defined before and  $n$  is the 2D density of the exciton gas. The effective mass of the exciton is taken to be  $m_X = 0.21m_e$ , where  $m_e$  is the free electron mass.<sup>46</sup> We assume that the healing length of a vortex in a four component BEC is comparable with one component BEC case.

We stress that the initial condition is used here only to set different topologies in the system. The final result of imaginary time propagation obtains the minimum energy state for a given topology (if such a state exists), that is, the ground state of a given topological defect characterized by winding numbers  $m_\sigma$ . We checked that such solutions are unchanged for different topologically invariant spatial profiles of the initial conditions; changing the specific shape of the radial wave function does not

change the final result. One could start the calculation with just uniform density subject to some circulation and the density dip of the vortex appears in the ground state results.

Note that the relative phases between the components in the initial condition (set by  $k_\sigma$ ) can affect the solution. Where this is so, we minimize over different values of  $k_\sigma$  to find the minimum energy state. Finally, we confirm that our results are stationary states by propagating them in real time numerically.

#### IV. VORTICES, HALF VORTICES, AND HALF VORTEX-ANTIVORTEX PAIRS

Let us first consider the cylindrically symmetric stationary wave function of the Gross-Pitaevskii equation as a possible minimal energy state for a rotating BEC around the  $z$ -axis,<sup>62</sup>

$$\Psi_\sigma(r, \theta, t) = R_\sigma(r) e^{i(m_\sigma \theta + k_\sigma \pi)} e^{-i\mu t}, \quad (12)$$

where  $\mu$  is the chemical potential of the condensate. The circulation of the tangential velocity over a closed contour for quantum vortices is quantized in units of  $2\pi\hbar/m_X$  controlled by the winding number  $m_\sigma$ , also known as *vorticity* or *topological charge*. Recent works on spinor exciton condensates have concluded that one of the simplest vortex solutions is of opposite vorticity in the  $\Psi_{\pm 1}$  components (half vortex-antivortex pair) and zero vorticity in the dark components (or vice versa).<sup>39,51</sup> This will later be shown to be indeed a possible low energy solution amongst other interesting vortex solutions for different  $m_\sigma$  and  $k_\sigma$ .

The radial part is taken to be purely real and is related to the total density of the condensate as

$$|R_{+1}|^2 + |R_{-1}|^2 + |R_{+2}|^2 + |R_{-2}|^2 = n, \quad (13)$$

where

$$\int \sum_\sigma |R_\sigma|^2 d^2r = N \quad (14)$$

is the total number of excitons in the system. In this paper we use the exciton density in the harmonic trap being  $n \propto 10^8 \text{ cm}^{-2}$ . The lateral size of the system of  $20 \mu\text{m}$  was chosen corresponding to localized bright spots observed in past experiments on exciton condensates.<sup>52</sup> The total number of particles was estimated as  $N \approx 100$ .

The phase difference  $k_\sigma \pi$  becomes essential in whether the vortex solution is present in the condensate or not. Adding  $\pi$  phase difference switches the sign of the wave function and thus switches the sign of the second line term in the nonlinear part of the Hamiltonian density [Eq. (5)] corresponding to bright to dark exciton conversion. Moreover, Eq. (12) reveals that for the solution to be cylindrically symmetric in the spinor exciton condensate the winding numbers need to satisfy the following

bound:

$$m_{+1} + m_{-1} = m_{+2} + m_{-2}. \quad (15)$$

Let us rewrite Eqs. (6)-(9), in the limit that the SOI strength is zero:

$$i\hbar \frac{\partial \Psi_{+2}}{\partial t} = \hat{E} \Psi_{+2} + V_0 n \Psi_{+2} + W \Psi_{-2}^* \Psi_{\Delta}^2, \quad (16)$$

$$i\hbar \frac{\partial \Psi_{+1}}{\partial t} = \hat{E} \Psi_{+1} + V_0 n \Psi_{+1} - W \Psi_{-1}^* \Psi_{\Delta}^2, \quad (17)$$

$$i\hbar \frac{\partial \Psi_{-1}}{\partial t} = \hat{E} \Psi_{-1} + V_0 n \Psi_{-1} - W \Psi_{+1}^* \Psi_{\Delta}^2, \quad (18)$$

$$i\hbar \frac{\partial \Psi_{-2}}{\partial t} = \hat{E} \Psi_{-2} + V_0 n \Psi_{-2} + W \Psi_{+2}^* \Psi_{\Delta}^2, \quad (19)$$

where we used definition  $\Psi_{\Delta}^2 \equiv \Psi_{+1} \Psi_{-1} - \Psi_{+2} \Psi_{-2}$ . Eqs. (16)-(19) show that the only difference between the equations describing bright and dark excitons is the sign of the  $W$  term describing bright to dark exciton conversion. This symmetry between bright and dark components means that if topological defects exist for the bright excitons then the same defects can exist for the dark excitons. Of main interest are configurations such as  $(m_{+2}, m_{+1}, m_{-1}, m_{-2}) = (0, 1, -1, 0), (1, 1, 1, 1), (1, 0, 1, 0)$  satisfying Eq. (15). We observe that if Eq. (15) is not satisfied, then there is no energy minimum for a trapped state of the considered topological defect, cylindrically symmetric or not. The real time propagation revealed that if for example a stable solution of  $m_\sigma = (0, 1, -1, 0)$  was suddenly switched to  $(0, 1, 1, 0)$  by conjugating the  $\Psi_{-1}$  component then the solution became immediately non-stationary and the localized topological defect was destroyed.

The vortices with high topological charges,  $|m_\sigma| > 1$ , were shown to be unstable in single component BECs depending on interaction strength.<sup>63</sup> This holds as well in our case: single topological defects are no longer observed for  $|m_\sigma| > 1$  in the case when SOI is absent. This situation changes, however, if SOI is taken into account as it will be discussed in the next section.

One should note that in the four component BEC the term vortex commonly applies when all components are rotating. The half vortex pair corresponds to circular motion of two components in the same direction, and half vortex-antivortex pair to two components with opposite direction of rotation.

In Fig. 2 we show four cases of low energy solutions for vortex topological defects in the four-component exciton condensate. The top plots correspond to a half vortex-antivortex pair in  $\Psi_{\pm 1}$ . The second from the top corresponds to a basic vortex composed of two half vortex-antivortex pairs in both bright and dark components. The second from the bottom corresponds to a basic vortex composed of two half vortex pairs in both bright and

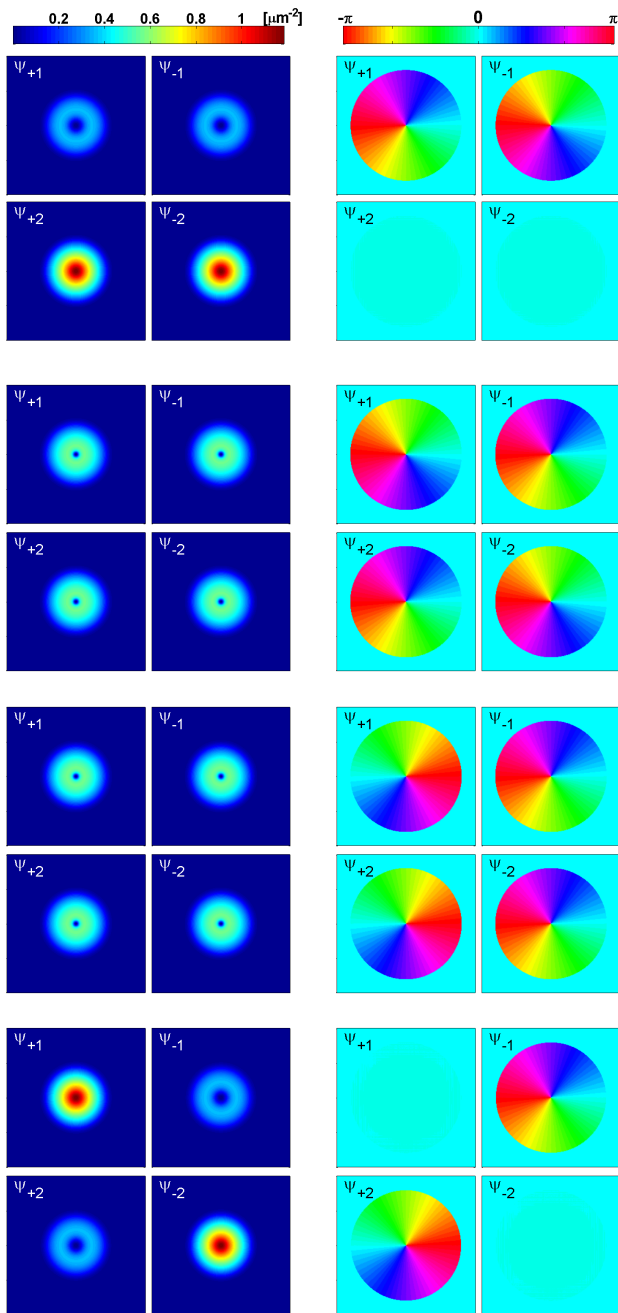


FIG. 2: (Color online) Density and phase profiles of the exciton condensate with different topological defects. **Top:**  $m_\sigma = (0, 1, -1, 0)$ . **Second from top:**  $m_\sigma = (1, -1, 1, -1)$ . **Second from bottom:**  $m_\sigma = (1, 1, 1, 1)$  and  $k_\sigma = (1, -1, 0, 0)$ . **Bottom:**  $m_\sigma = (1, 0, 1, 0)$  and  $k_\sigma = (1, 0, 0, 0)$ . In the top three:  $V_0 = 1$  and  $W = -0.1 \mu\text{eV}\mu\text{m}^{-2}$ . Bottom:  $V_0 = 1$  and  $W = 0.1 \mu\text{eV}\mu\text{m}^{-2}$ . In all pictures:  $u_0 = 1 \mu\text{eV}\mu\text{m}^{-2}$ .

dark components — both with a  $\pi$  phase difference. Bottom plots correspond to a half vortex pair in  $\Psi_{-1}$  and  $\Psi_{+2}$  components. One can see in the top and bottom lines that the vortex core stabilizes at a greater healing length due to the other components trying to fill in

the density dips. The densities of bright and dark excitons try to complement each other, staying close to the Thomas-Fermi profile.

The existence of a low energy solution with vortices is determined by the last term in Eqs. (16)-(19) and the kinetic energy term. This can be seen from analysis of the Hamiltonian density (5). In the case of  $W = 0$  there is a competition between the kinetic energy term in the total Hamiltonian and the interaction energy term

$$\mathcal{H}_{\text{int}} = \frac{V_0}{2} (|\Psi_{+2}|^2 + |\Psi_{+1}|^2 + |\Psi_{-1}|^2 + |\Psi_{-2}|^2)^2.$$

If interactions are weak then it will be energetically favorable to transfer intensity from a component with a vortex to a component without one, since a component with a vortex has higher kinetic energy. For this reason, there may be no minimal energy states with vortices in two components only — numerical calculations give instead a depletion of components containing vortices in favor of those without vortices. We can then expect that the only possible stable states with non-zero topological charges (in components with non-zero intensity) contain vortices in all components.

One should keep in mind that while the kinetic energy contribution can be reduced by transferring intensity to a component without a vortex, this may increase the potential energy due to interactions. The term proportional to  $V_0$  in the Hamiltonian can be reduced if the spatial overlap of the intensity distribution of components is reduced. Thus the  $V_0$  term favors formation of vortices, but it must be strong enough to overcome the corresponding increase of kinetic energy for the states with vortices in two components only.

In the case  $W \neq 0$  and  $(m_{+2}, m_{+1}, m_{-1}, m_{-2}) = (0, 1, -1, 0)$  the wave functions can be written:

$$\Psi_{+2} = U(r)e^{i\phi_{+2}}, \quad \Psi_{+1} = V(r)e^{i\theta}e^{i\phi_{+1}}$$

$$\Psi_{-1} = V(r)e^{-i\theta}e^{i\phi_{-1}}, \quad \Psi_{-2} = U(r)e^{i\phi_{-2}}$$

where  $U(r)$  and  $V(r)$  are real functions. The  $W$  dependent part of the Hamiltonian can then be written as

$$\mathcal{H}_W = W [2U^2V^2 \cos(\Delta\phi) - U^4 - V^4], \quad (20)$$

where  $\Delta\phi = \phi_{+2} + \phi_{-2} - \phi_{+1} - \phi_{-1}$ .

In the case that  $W > 0$ , the phases can be chosen to minimize the Hamiltonian to  $\mathcal{H}_W = -W(U^2 + V^2)^2 = -W(|\Psi_{+2}|^2 + |\Psi_{+1}|^2 + |\Psi_{-1}|^2 + |\Psi_{-2}|^2)^2$ . That is, the  $W$  term has the same form as the  $V_0$  term. Consequently, the same arguments as considered in the  $W = 0$  case apply: if the strength of the interaction  $V_0 - W$  is unable to overcome the kinetic energy term, then a state with vortices in two components only (with non-zero intensity) is not stable.

In the case that  $W < 0$ , the phase can be chosen to minimize the Hamiltonian to  $\mathcal{H}_W = -W(U^2 - V^2)^2$  (a

positive quantity since  $W < 0$ ). This term favors states with vortices in two components (see Fig. 2, top case) since it is minimized if all components stay populated.

Note that it is not possible to say definitively whether vortices will or will not be stable for the cases where  $W$  is positive or negative without use of numerical calculation because of the tricky interplay between potential and kinetic energy terms.

In the case of  $W \neq 0$  and  $(m_{+2}, m_{+1}, m_{-1}, m_{-2}) = (1, 0, 1, 0)$  the wave functions can be written:

$$\Psi_{+2} = V(r)e^{i\theta}e^{i\phi_{+2}}, \quad \Psi_{+1} = U(r)e^{i\phi_{-1}}$$

$$\Psi_{-1} = V(r)e^{i\theta}e^{i\phi_{+1}}, \quad \Psi_{-2} = U(r)e^{i\phi_{-2}}.$$

The  $W$  dependent part of the Hamiltonian density is

$$\mathcal{H}_W = 2WU^2V^2 [\cos(\Delta\phi) - 1]. \quad (21)$$

In the case  $W > 0$ , the phases can be chosen to minimize the Hamiltonian to  $\mathcal{H}_W = -4WU^2V^2$ . This term may stabilize the state, since it provides a reduction of the energy when all components are populated (see Fig. 2, bottom case); if one component is depleted then this term can no longer contribute to minimization of the energy.

In the case  $W < 0$ , the phases can be chosen to minimize the Hamiltonian to  $\mathcal{H}_W = 0$ . In this case we recover the result for the  $W = 0$  case. While it is not possible to say definitively whether vortices will be stable for the  $W > 0$ , we can say that for  $W < 0$  they are unstable if they are also unstable for the  $W = 0$  case.

## V. CYLINDRICALLY SYMMETRIC GROUND STATE SOLUTIONS UNDER SPIN-ORBIT INTERACTION

When SOI of Rashba or/and Dresselhaus type is included in the Hamiltonian, the analysis of low energy state solutions becomes more tricky. Prior studies in the field of atomic condensates revealed a plethora of phenomena emerging due to spin-orbit coupling.<sup>13,17</sup> Indirect exciton condensates can be expected to show also a great variety in possible low energy solutions with phase separation between components and density modulations.

Let us first analyze the possibility of the cylindrically symmetric solutions. Using the ansatz  $\Psi_\sigma = R_\sigma(r)e^{im_\sigma\theta}$  in Eqs. (6)-(9) we find that if only Dresselhaus SOI is present, the winding numbers should satisfy the following bound [in addition to those given by Eq. (15)]:

$$\begin{aligned} m_{+2} &= 1 + n, & m_{+1} &= n, \\ m_{-1} &= 1 + m, & m_{-2} &= m. \end{aligned} \quad (22)$$

On the other hand, if only Rashba SOI is present the bound is:

$$\begin{aligned} m_{+2} &= n, & m_{+1} &= 1 + n, \\ m_{-1} &= m, & m_{-2} &= 1 + m, \end{aligned} \quad (23)$$

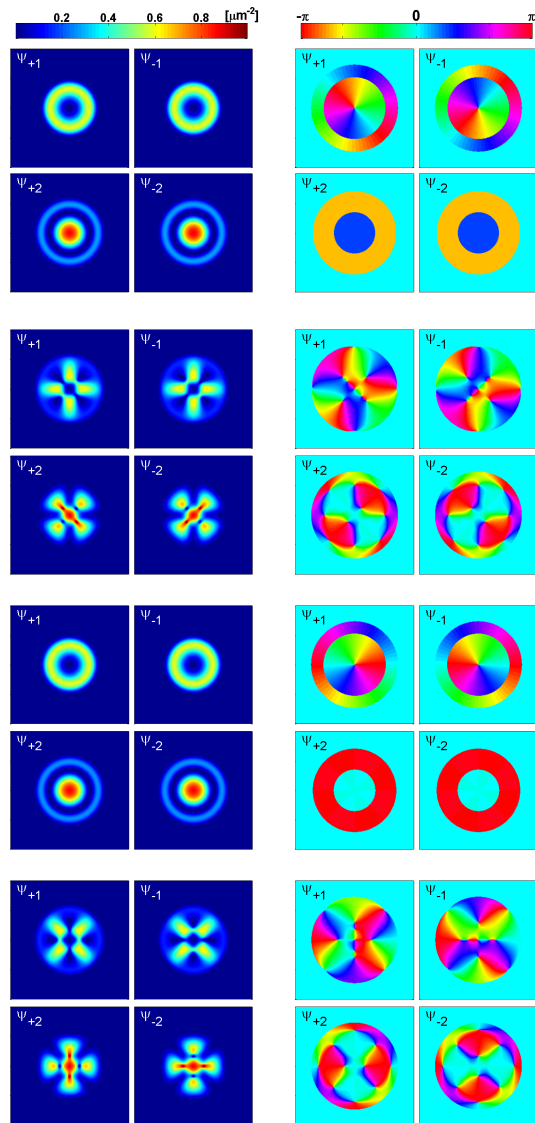


FIG. 3: (Color online) The difference between Dresselhaus and Rashba SOI displayed. Density and phase profiles of the condensate components with different vortex defects as initial condition. In the top two cases:  $\beta = 1 \mu\text{eV}\mu\text{m}$  and  $\alpha = 0$ . In the lower two cases:  $\beta = 0$  and  $\alpha = 1 \mu\text{eV}\mu\text{m}$ . **Top:**  $\beta = 1 \mu\text{eV}\mu\text{m}$  and  $\alpha = 0$ , initial configuration corresponds to  $m_\sigma = (0, -1, 1, 0)$ . The bound (22) is satisfied and cylindrically symmetric vortex type solution is obtained. **Second from top:**  $\beta = 1 \mu\text{eV}\mu\text{m}$  and  $\alpha = 0$ ,  $m_\sigma = (0, 1, -1, 0)$ . The bound (22) is not satisfied, and as a result warped vortex corresponding to  $m_\sigma = (+2, +3, -3, -2)$  is formed in a stationary regime. **Second from bottom:**  $\beta = 0$  and  $\alpha = 1 \mu\text{eV}\mu\text{m}$ ,  $m_\sigma = (0, 1, -1, 0)$ . The bound (23) is satisfied and cylindrically symmetric vortex type solution is obtained. **Bottom:**  $\beta = 0$  and  $\alpha = 1 \mu\text{eV}\mu\text{m}$ , initial configuration corresponds to  $m_\sigma = (0, -1, 1, 0)$ . The bound (23) is not satisfied, and as a result warped vortex corresponding to  $m_\sigma = (-2, -3, +3, +2)$  is formed in stationary regime. In all pictures:  $k_\sigma = (0, 0, 0, 0)$ ,  $V_0 = 22 \mu\text{eV}\mu\text{m}^{-2}$ ,  $W = 2 \mu\text{eV}\mu\text{m}^{-2}$  and  $u_0 = 1 \mu\text{eV}\mu\text{m}^{-2}$ .

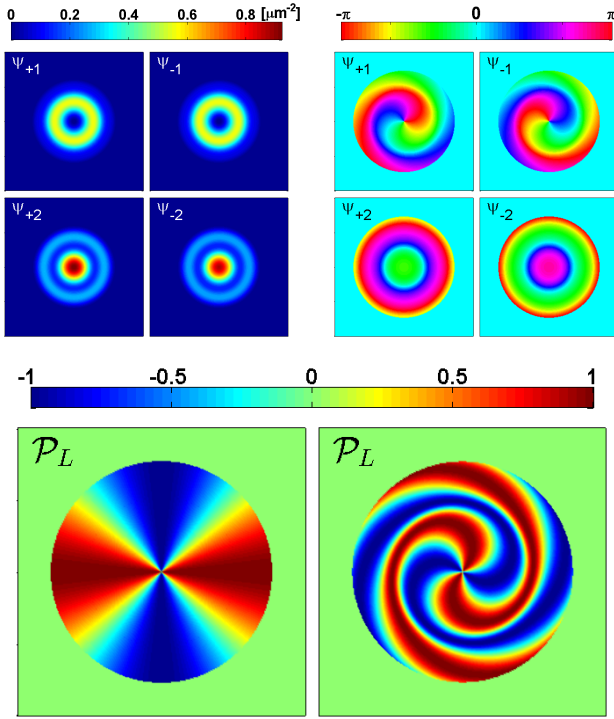


FIG. 4: (Color online) **Top:** Density and phase profiles of the exciton condensate components for only Dresselhaus SOI.  $m_\sigma = (0, -1, 1, 0)$ ,  $k_\sigma = (0, 1, 0, 0)$  and  $W = 2 \mu\text{eV}\mu\text{m}^{-2}$ ,  $V_0 = 28 \mu\text{eV}\mu\text{m}^{-2}$ ,  $\beta = 1 \mu\text{eV}\mu\text{m}$  and  $u_0 = 1 \mu\text{eV}\mu\text{m}^{-2}$ . **Bottom:** Linear polarization of cylindrically symmetric cases for Dresselhaus SOI only with  $m_\sigma = (0, -1, 1, 0)$  initial condition. The **right** panel was calculated for  $k_\sigma = (0, 0, 0, 0)$ , and corresponds to the top panel in Fig. 3. For the **left** panel we set  $k_\sigma = (0, 1, 0, 0)$ , corresponding to the top panel in this figure.

where  $n$  and  $m$  are integer numbers.

We limit our consideration in this section of the paper to three types of cylindrical vortex configurations for SOI of either Dresselhaus or Rashba type:  $m_\sigma = (0, 1, -1, 0)$ ,  $(0, -1, 1, 0)$ , and  $(1, 0, 1, 0)$ . We show that in the case where the bounds (22) or (23) are not satisfied the initial topological charge is not preserved but instead the configuration of *warped vortices* with winding numbers greater than one,  $m_\sigma = (\pm 2, \pm 3, \mp 3, \mp 2)$ ,<sup>6</sup> or density modulated stripe phase with no vorticity is established, depending on the initial conditions.

For Dresselhaus SOI only the configurations  $m_\sigma = (0, -1, 1, 0)$  and  $(1, 0, 1, 0)$  satisfy Eq. (22), and we observe formation of the cylindrically symmetric vortices (Fig. 3 top and Fig. 6), whereas  $m_\sigma = (0, 1, -1, 0)$  does not satisfy the bound, the cylindrical symmetry is no longer present, and configuration with higher winding numbers  $m_\sigma = (+2, +3, -3, -2)$  is formed (Fig. 3, second from top). The similar behavior can be observed for the case of the Rashba SOI but this time the cylindrical symmetry is manifested for  $m_\sigma = (0, 1, -1, 0)$  and  $(0, 1, 0, 1)$  configurations.

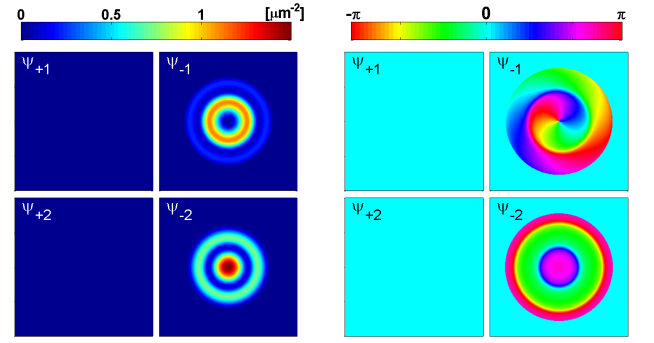


FIG. 5: (Color online) Density and phase profiles of the exciton condensate components for only Dresselhaus SOI.  $m_\sigma = (0, -1, 1, 0)$ ,  $k_\sigma = (0, 0, 0, 0)$ ,  $W = -2 \mu\text{eV}\mu\text{m}^{-2}$ ,  $V_0 = 28 \mu\text{eV}\mu\text{m}^{-2}$ ,  $\beta = 1 \mu\text{eV}\mu\text{m}$  and  $u_0 = 1 \mu\text{eV}\mu\text{m}^{-2}$ .

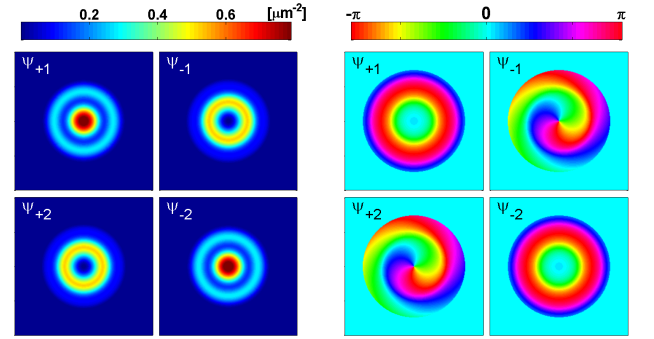


FIG. 6: (Color online) Density and phase profiles of the exciton condensate half vortex pair for only Dresselhaus SOI.  $m_\sigma = (1, 0, 1, 0)$ ,  $k_\sigma = (0, 0, 0, 0)$ ,  $V_0 = 28 \mu\text{eV}\mu\text{m}^{-2}$ ,  $W = \pm 2 \mu\text{eV}\mu\text{m}^{-2}$ ,  $\beta = 1 \mu\text{eV}\mu\text{m}$  and  $u_0 = 1 \mu\text{eV}\mu\text{m}^{-2}$ .

Fig. 3 shows stable solutions for the half vortex-antivortex configurations  $m_\sigma = (0, 1, -1, 0)$ , and  $(0, -1, 1, 0)$ . The top two panels correspond to the case when only Dresselhaus SOI is present and the bottom two for the case when only Rashba SOI is present. Inspecting the phase profiles (top and second from bottom panel) reveals that phases of the components are different for the cases of Dresselhaus and Rashba SOI: there is a  $3\pi/4$  phase difference in  $\Psi_{+1}$ ,  $-\pi/4$  difference in  $\Psi_{-1}$  and  $\pi/4$  difference in  $\Psi_{\pm 2}$  amplitudes if one changes Dresselhaus SOI to Rashba. These phase differences result in the  $\pi/2$  rotation of the pattern of the linear polarization degree calculated as

$$\mathcal{P}_L = \frac{\Psi_{+1}^* \Psi_{-1} + \Psi_{-1}^* \Psi_{+1}}{|\Psi_{+1}|^2 + |\Psi_{-1}|^2} \propto \cos(2\theta) \quad (24)$$

if one switches from Rashba to Dresselhaus SOI. The result is expectable, as the operator describing Rashba SOI can be obtained from the operator describing Dresselhaus SOI by switching  $K_x$  to  $K_y$  and vice versa [see Eq. (4)].

We observe that in the cylindrically symmetric case

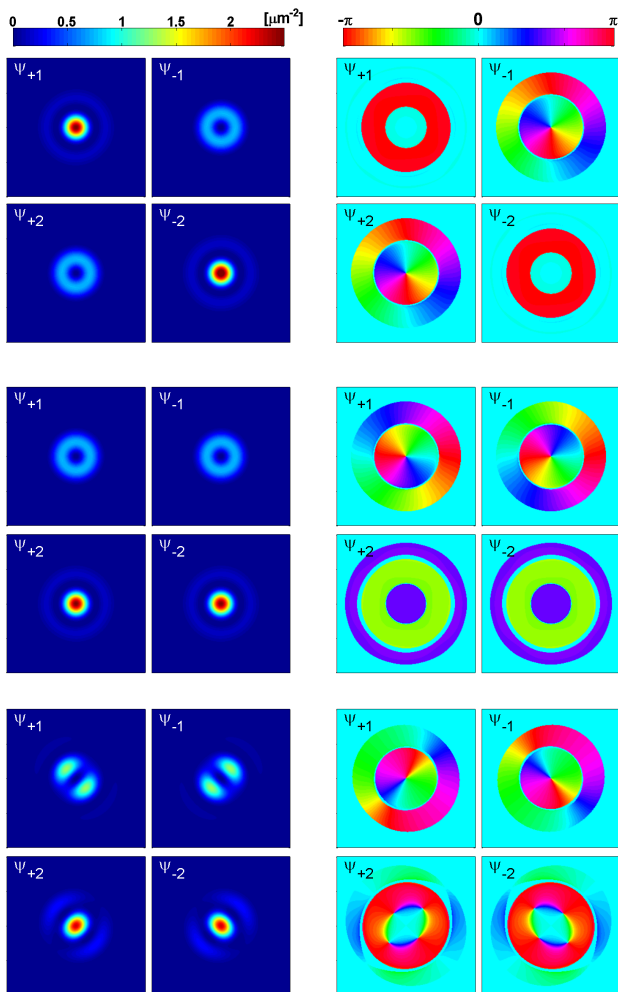


FIG. 7: (Color online) Density and phase profiles of the exciton condensate components for only Dresselhaus SOI and small nonlinear parameters. **Top:**  $m_\sigma = (1, 0, 1, 0)$ . **Middle:**  $m_\sigma = (0, -1, 1, 0)$ . **Bottom:**  $m_\sigma = (0, 1, -1, 0)$ . In all pictures the parameters were  $\beta = 1 \mu\text{eV}\mu\text{m}$ ,  $V_0 = 2.8 \text{ neV}\mu\text{m}^{-2}$ ,  $W = \pm 0.2 \text{ neV}\mu\text{m}^{-2}$  and  $u_0 = 1 \text{ neV}\mu\text{m}^{-2}$ .

there are two alternative configurations of the vortex corresponding to the same combination of the winding numbers. One of them is demonstrated in Fig. 3 and corresponds to the case when the phase of macroscopic wavefunction depends only on the angle  $\phi$ . This solution is obtained if all  $k_\sigma$  are put to zero. However, if one introduces phase difference between the condensate components chosen as an initial condition (i.e.  $k_\sigma \neq 0$ ), another type of the vortex solution corresponding to the spiral phase pattern is obtained [see Fig. 4, top]. The topological charges of both solutions are the same, and to distinguish between them one needs to analyze their linear polarization patterns shown in Fig. 4 (bottom). As one can see, they are radically different, being four leaf in one case and gammadion in the other.

Also we note that the sign of exchange interaction  $W$  affects the possible states of stable topological defects.

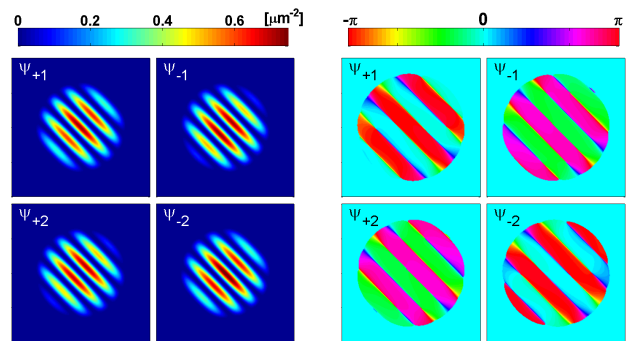


FIG. 8: (Color online) Density and phase profile of condensate components for  $m_\sigma = (0, 0, 0, 0)$  and  $k_\sigma = (0, 1, 0, 0)$ , the parameters were  $\beta = 1 \mu\text{eV}\mu\text{m}$ ,  $\alpha/\beta = 1/2$ ,  $V_0 = 28 \mu\text{eV}\mu\text{m}^{-2}$  and  $W = -2 \mu\text{eV}\mu\text{m}^{-2}$ .

To illustrate its role, we focus on a configuration  $m_\sigma = (0, -1, 1, 0)$  (same as in top panel in Fig. 3) and set the parameters to:  $\beta = 1 \mu\text{eV}\mu\text{m}$ ,  $\alpha = 0$  and  $W = -2 \mu\text{eV}\mu\text{m}^{-2}$ . We observe a half vortex in a condensate half depleted with a spiral phase pattern resulting from negative  $W$  [see Fig. 5]. The results are clearly different from those shown in Fig. 3 corresponding to opposite sign of the exchange interaction,  $W = +2 \mu\text{eV}\mu\text{m}^{-2}$ .

In Fig. 6 we show a half vortex pair solution with  $m_\sigma = (1, 0, 1, 0)$  for only Dresselhaus SOI [in case of only Rashba it would be  $m_\sigma = (0, 1, 0, 1)$ ]. The solution remained the same for both signs of the mixing parameter  $W$  and was lost when  $k_\sigma \neq 0$ .

We also investigated the ground state vortex solutions for the case when the nonlinearities are very weak and the impact of the SOI terms becomes dominant ( $V_0, W \ll \beta, \alpha$ ). Fig. 7 illustrates the case when only Dresselhaus SOI is present. If the bound (22) is satisfied the solutions have cylindrical symmetry (top two panels). For the case  $m_\sigma = (0, 1, -1, 0)$  the solution is non-symmetric and resembles a hybrid of a warped vortex solution and a striped phase. In this weakly nonlinear limit the sign of  $W$  becomes irrelevant, and the same patterns were observed for  $W = \pm 0.2 \text{ neV}\mu\text{m}^{-2}$ .

## VI. PRESENCE OF BOTH DRESSELHAUS AND RASHBA SOI

When both  $\alpha \neq 0$  and  $\beta \neq 0$  the single particle spectrum becomes anisotropic. Different from the cases  $\alpha = 0$  or  $\beta = 0$  the minima of the energy of non-interacting particles correspond not to a circle of constant radius in the reciprocal space, but to the two fixed points situated along  $K_x$ - $K_y$  diagonal,<sup>64</sup>

$$\mathbf{K}_0 = \pm \frac{\chi m_X (\alpha + \beta)}{\hbar^2} \frac{(\mathbf{e}_x + \mathbf{e}_y)}{\sqrt{2}}. \quad (25)$$

One can thus expect formation of a striped ground state corresponding to the spatial modulation of the density



$(e^{i\mathbf{K}_0 \cdot \mathbf{r}} + e^{-i\mathbf{K}_0 \cdot \mathbf{r}}) = 2 \cos(\mathbf{K}_0 \cdot \mathbf{r})$ . This is indeed the case as can be seen in Fig. 8. As the ground state of the condensate reveals spatial anisotropy, no cylindrically symmetric vortex solutions can be expected to appear in this case.

The stability of the vortex-type versus striped phase solutions depends on the ratio  $\alpha/\beta$ . Fixing the parameters describing nonlinearities as  $V_0 = 28 \mu\text{eV}\mu\text{m}^{-2}$  and  $W = \pm 2 \mu\text{eV}\mu\text{m}^{-2}$ , our numerical analysis shows that for  $\alpha/\beta \sim 10^{-3}$  the vortex type solutions shown in Figs. 3-6 still persist. However, already at  $\alpha/\beta \sim 10^{-2}$  all vortex solutions disappear and only stripe phase solutions are stable. This is illustrated in Fig. 8, where we have set  $\beta = 1 \mu\text{eV}\mu\text{m}$  and  $\alpha/\beta = 1/2$  for a spatially uniform condensate as a initial condition of the imaginary time method.

## VII. CONCLUSIONS

We studied the stationary solutions describing various topological defects in the system of spinor indirect ex-

citons applying the imaginary time method to the set of Gross-Pitaevskii equations. We analyzed the role of the SOI of Rashba and Dresselhaus types in formation of single vortices, half vortices and half vortex-antivortex pairs, and described the transition between warped vortex and stripe phase solutions in the presence of both Rashba and Dresselhaus SOI.

*Acknowledgements.* We thank Yuri G. Rubo and Alexey V. Kavokin for the valuable discussions. This work was supported by FP7 IRSES projects SPINMET and POLAPHEN and Tier 1 project ‘‘Polaritons for novel device applications’’. O. K. acknowledges the support from Eimskip Fund. H. S. thanks Universidad Autonoma de Mexico for hospitality.

- 
- <sup>1</sup> M. H. Anderson, J. R. Ensher, M. R. Matthews, C. E. Wieman, and E. A. Cornell, *Science* **269**, 198 (1995).
  - <sup>2</sup> K. B. Davis, M.-O. Mewes, M. R. Andrews, N. J. van Druten, D. S. Durfee, D. M. Kurn, and W. Ketterle, *Phys. Rev. Lett.* **75**, 3969 (1995).
  - <sup>3</sup> M. R. Matthews, B. P. Anderson, P. C. Haljan, D. S. Hall, C. E. Wieman, and E. A. Cornell, *Phys. Rev. Lett.* **83**, 2498 (1999).
  - <sup>4</sup> L. Pitaevskii and S. Stringari, *Bose-Einstein Condensation* (Oxford University Press, Oxford, 2003) and A. Leggett, *Quantum Liquids: Bose Condensation and Cooper Pairing in Condensed-Matter Systems* (Oxford University Press, Oxford, 2006).
  - <sup>5</sup> Y. S. Kivshar and G. Agrawal, *Optical Solitons: From Fibers to Photonic Crystals* (Academic Press, USA, 2003).
  - <sup>6</sup> M. Toledo Solano and Y. G. Rubo *Phys. Rev. B* **82**, 127301 (2010).
  - <sup>7</sup> U. Al Khawaja and H. Stoof, *Nature* **411**, 918 (2001).
  - <sup>8</sup> E. Babaev, *Phys. Rev. Lett.* **89**, 067001 (2002).
  - <sup>9</sup> D. Vollhardt and P. Wölfle, *The Superfluid Phases of Helium 3* (Taylor & Francis, London, 1990).
  - <sup>10</sup> K. W. Madison, F. Chevy, W. Wohlleben, and J. Dalibard, *Phys. Rev. Lett.* **84**, 806 (2000).
  - <sup>11</sup> J. R. Abo-Shaer, C. Raman, J. M. Vogels, and W. Ketterle, *Science* **292**, 476 (2001).
  - <sup>12</sup> Y.-J. Lin, R. L. Compton, K. Jimenez-Garcia, J. V. Porto, and I. B. Spielman, *Nature* **462**, 628 (2009).
  - <sup>13</sup> Y.-J. Lin, K. Jiménez-García, and I. B. Spielman, *Nature* **471**, 83 (2011).
  - <sup>14</sup> T. D. Stanescu, B. Anderson, and V. Galitski, *Phys. Rev. A* **78**, 023616 (2008).
  - <sup>15</sup> C. Wu, I. Mondragon-Shem, and X.-F. Zhou, *Chin. Phys. Lett.* **28**, 097102 (2011).
  - <sup>16</sup> B. Ramachandhran, B. Opanchuk, X.-J. Liu, H. Pu, P. D. Drummond, and H. Hu, *Phys. Rev. A* **85**, 023606 (2012).
  - <sup>17</sup> V. Galitski and I. B. Spielman, *Nature* **494**, 49 (2013).
  - <sup>18</sup> C. Wang, C. Gao, C.-M. Jian, and H. Zhai, *Phys. Rev. Lett.* **105**, 160403 (2010).
  - <sup>19</sup> S. Sinha, R. Nath, and L. Santos, *Phys. Rev. Lett.* **107**, 270401 (2011).
  - <sup>20</sup> E. Ruokokoski, J. A. M. Huhtamäki, and M. Möttönen, *Phys. Rev. A* **86**, 051607(R) (2012).
  - <sup>21</sup> Hui Hu, B. Ramachandhran, Han Pu, and Xia-Ji Liu, *Phys. Rev. Lett.* **108**, 010402 (2012).
  - <sup>22</sup> S. Gopalakrishnan, I. Martin, and E. A. Demler, *Phys. Rev. Lett.* **111**, 185304 (2013).
  - <sup>23</sup> I. B. Spielman, J. P. Eisenstein, L. N. Pfeiffer, and K. W. West, *Phys. Rev. Lett.* **87**, 036803 (2001); J. P. Eisenstein and A. H. MacDonald, *Nature* **432**, 691 (2004).
  - <sup>24</sup> S. O. Demokritov, V. E. Demidov, O. Dzyapko, G. A. Melkov, A. A. Serga, B. Hillebrands, A. N. Slavin, *Nature* **443**, 430 (2006).
  - <sup>25</sup> L. V. Butov et al., *Phys. Rev. Lett.* **86**, 5608 (2001).
  - <sup>26</sup> D. Snoke, *Science* **298**, 1368 (2002).
  - <sup>27</sup> A. A. High, J. R. Leonard, A. T. Hammack, M. M. Fogler, L. V. Butov, A. V. Kavokin, K. L. Campman, and A. C. Gossard, *Nature* **483**, 584 (2012).
  - <sup>28</sup> J. Kasprzak, M. Richard, S. Kundermann, A. Baas, P. Jeambrun, J. M. J. Keeling, F. M. Marchetti, M. H. Szymanska, R. Andre, J. L. Staehli, V. Savona, P. B. Littlewood, B. Deveaud, and Le Si Dang, *Nature* **443**, 409 (2006).
  - <sup>29</sup> R. Balili, V. Hartwell, D. Snoke, L. Pfeiffer, and K. West, *Science* **316**, 1007 (2007).
  - <sup>30</sup> J. J. Baumberg, A. V. Kavokin, S. Christopoulos, A. J. D. Grundy, R. Butté, G. Christmann, D. D. Solnyshkov, G. Malpuech, G. Baldassarri Höger von Hogerthal, E. Feltn, J.-F. Carlin, and N. Grandjean, *Phys. Rev. Lett.* **101**, 136409 (2008).
  - <sup>31</sup> C. Schneider, A. Rahimi-Iman, Na Young Kim, J. Fis-

- cher, I. G. Savenko, M. Amthor, M. Lermer, A. Wolf, L. Worschech, V. D. Kulakovskii, I. A. Shelykh, M. Kamp, S. Reitzenstein, A. Forchel, Y. Yamamoto, and S. Hofling, *Nature* **497**, 348 (2013).
- <sup>32</sup> I. A. Shelykh, A. V. Kavokin, Yu. G. Rubo, T. C. H. Liew, and G. Malpuech, *Semicond. Sci. Technol.* **25**, 013001 (2010).
- <sup>33</sup> K. G. Lagoudakis, M. Wouters, M. Richard, A. Baas, I. Carusotto, R. André, Le Si Dang, and B. Deveaud-Plédran, *Nature Phys.* **4**, 706 (2008).
- <sup>34</sup> T. C. H. Liew, Y. G. Rubo, and A. V. Kavokin, *Phys. Rev. Lett.* **101**, 187401 (2008).
- <sup>35</sup> K. G. Lagoudakis, F. Manni, B. Pietka, M. Wouters, T. C. H. Liew, V. Savona, A. V. Kavokin, R. André, and B. Deveaud-Plédran, *Phys. Rev. Lett.* **106**, 115301 (2011).
- <sup>36</sup> Y. G. Rubo, *Phys. Rev. Lett.* **99**, 106401 (2007).
- <sup>37</sup> K. G. Lagoudakis, T. Ostatnický, A. V. Kavokin, Y. G. Rubo, R. André, and B. Deveaud-Plédran, *Science* **326**, 974 (2009).
- <sup>38</sup> F. Manni, K. G. Lagoudakis, T. C. H. Liew, R. André, V. Savona, and B. Deveaud, *Nature Commun.* **3**, 1309 (2012).
- <sup>39</sup> H. Flayac, I. A. Shelykh, D. D. Solnyshkov, and G. Malpuech, *Phys. Rev. B* **81**, 045318 (2010).
- <sup>40</sup> I. A. Shelykh, Yuri G. Rubo, G. Malpuech, D. D. Solnyshkov, and A. Kavokin, *Phys. Rev. Lett.* **97**, 066402 (2006).
- <sup>41</sup> T. C. H. Liew, A. V. Kavokin, and I. A. Shelykh, *Phys. Rev. B* **75**, 241301(R) (2007).
- <sup>42</sup> F. Manni, K. G. Lagoudakis, T. K. Paraíso, R. Cerna, Y. Léger, T. C. H. Liew, I. A. Shelykh, A. V. Kavokin, F. Morier-Genoud, and B. Deveaud-Plédran, *Phys. Rev. B* **83**, 241307(R) (2011).
- <sup>43</sup> Yu. E. Lozovik and V. I. Yudson, *Zh. Eksp. Teor. Fiz. Pisma Red.* **22**, 26 (1975) [*JETP Lett.* **22**, 26 (1975)]; *Zh. Eksp. Teor. Fiz.* **71**, 738 (1976) [*Sov. Phys. JETP* **44**, 389 (1976)]; *Solid State Commun.* **18**, 628 (1976).
- <sup>44</sup> V. B. Timofeev, *Physics-Uspekhi* **48**, 295 (2005).
- <sup>45</sup> L. V. Butov, *J. Phys. Condens. Matter* **19**, 295202 (2007).
- <sup>46</sup> L. V. Butov, C. W. Lai, A. L. Ivanov, A. C. Gossard, and D. S. Chemla, *Nature* **417**, 47 (2002); L. V. Butov, A. C. Gossard, and D. S. Chemla, *Nature* **418**, 751 (2002).
- <sup>47</sup> D. Snoke, S. Denev, Y. Liu, L. Pfeiffer, and K. West, *Nature* **418**, 754 (2002).
- <sup>48</sup> M. Alloing, D. Fuster, Y. González, L. González, and F. Dubin, arXiv:1210.3176 (2012).
- <sup>49</sup> Yu. G. Rubo and A. V. Kavokin, *Phys. Rev. B* **84**, 045309 (2011).
- <sup>50</sup> O. Kyriienko, E. B. Magnusson, and I. A. Shelykh, *Phys. Rev. B* **86**, 115324 (2012).
- <sup>51</sup> M. Matuszewski, T. C. H. Liew, Y. G. Rubo, and A. V. Kavokin, *Phys. Rev. B* **86**, 115321 (2012).
- <sup>52</sup> A. A. High, A. T. Hammack, J. R. Leonard, S. Yang, L. V. Butov, T. Ostatnický, M. Vladimirova, A. V. Kavokin, T. C. H. Liew, K. L. Campman, and A. C. Gossard, *Phys. Rev. Lett.* **110**, 246403 (2013).
- <sup>53</sup> D. V. Vishnevsky, H. Flayac, A. V. Nalitov, D. D. Solnyshkov, N. A. Gippius, and G. Malpuech, *Phys. Rev. Lett.* **110**, 246404 (2013).
- <sup>54</sup> A. V. Kavokin, M. Vladimirova, B. Jouault, T. C. H. Liew, J. R. Leonard, and L. V. Butov, arXiv:1305.0133 (2013).
- <sup>55</sup> K. B. Arnardottir, O. Kyriienko, and I. A. Shelykh, *Phys. Rev. B* **86**, 245311 (2012).
- <sup>56</sup> M. Z. Maialle, E. A. de Andrada e Silva, L. J. Sham, *Phys. Rev. B* **47**, 15776 (1993).
- <sup>57</sup> M. Combescot, O. Betbeder-Matibet, and R. Combescot, *Phys. Rev. Lett.* **99**, 176403 (2007).
- <sup>58</sup> R. Combescot and M. Combescot, *Phys. Rev. Lett.* **109**, 026401 (2012).
- <sup>59</sup> M. A. Can and T. Hakioglu, *Phys. Rev. Lett.* **103**, 086404 (2009).
- <sup>60</sup> M. Combescot, O. Betbeder-Matibet, and F. Dubin, *Physics Reports* **463**, 215 (2008).
- <sup>61</sup> M. Combescot, O. Betbeder-Matibet, and R. Combescot, *Phys. Rev. B* **75**, 174305 (2007).
- <sup>62</sup> A. Fetter and A. Svidzinsky, *J. Phys. Condens. Matter* **13**, R135 (2001).
- <sup>63</sup> H. Pu, C. K. Law, J. H. Eberly and N. P. Bigelow, *Phys. Rev. A* **59**, 1533 (1999).
- <sup>64</sup> R. H. Silsbee, *J. Phys. Condens. Matter* **16**, R179 (2004).